Science
AAAS

Supplementary Materials for

A plant lipocalin promotes retinal-mediated oscillatory lateral root initiation

Alexandra J. Dickinson *et al.*

Corresponding authors: Alexandra J. Dickinson, adickinson@ucsd.edu; Philip N. Benfey, philip.benfey@duke.edu

Science **373**, 1532 (2021)
DOI: 10.1126/science.abf7461

The PDF file includes:

Other Supplementary Material for this manuscript includes the following:

Materials and Methods

Plant Growth and Treatment Conditions

All *Arabidopsis thaliana* plants were in the Columbia-0 background. Null mutants *til-1* (SALK_136775C) and *til-2* (SALK_150259C) were obtained from the ABRC. Retinal, apo-14, and apo-12 were generously supplied by Earl Harrison (Ohio State University). Apo-10 was generously supplied by Loredana Quadro (Rutgers). Working concentrations of retinal and apo-14 for long term (> 24 hour) experiments were 1 mM and 500 nM, respectively. For long term experiments, plates were wrapped in parafilm and the roots were grown on treated media and kept in the dark. For these experiments, the shoots were not directly treated with media and were the only part of the plant exposed to light. The merocyanine aldehyde (MCA) used is related to a previously described compound *(13)*, see supplemental information for a full description of the synthesis and characterization of the aldehyde and putative chromophore formed.

Root Phenotyping

Merocyanine aldehyde (MCA) was synthesized as previously described *(13)*. To measure MCA fluorescence in plants, roots were treated with 10 mM MCA and imaged using dsRED filter sets. Fluorescence was tracked over time via stereomicroscopy or confocal microscopy. Lateral root capacity, or the ability of the plant to produce lateral roots, was measured as described previously[1]. Briefly, the root meristems were excised 5 days post-germination. This induces lateral root emergence. Three days after excision, the total number of emerged lateral roots was quantified. Lateral root clock oscillations were characterized using time-lapse imaging as previously described by Moreno-Risueno *et al*. Roots were sprayed with 5 mM potassium luciferine (Gold Biotechnology) and then were imaged every 7 min over the course of 18 h using a chemiluminescence imaging system (Roper Bioscience).

Chemical Analysis

HPLC-MS samples were prepared by homogenizing whole seedlings 5 days post germination in liquid nitrogen. Apocarotenoids were extracted from 100-200 mg of homogenized root tissue using propanol with 0.1% butylated hydroxytoluene. LC-MS/MS was performed using an Agilent 1260 HPLC coupled to an Agilent 6520 Q-TOF ESI mass spectrometer. Separation was conducted in a 5 μm, 2 × 100 mm Gemini NX-C18 column (Phenomenex). The mobile phase solvents used were water with 0.1% (v/v) formic acid (Solvent A) and acetonitrile with 0.1% (v/v) formic acid (Solvent B). A linear gradient with a flow rate of 0.4 mL/min was used over the course of the separation. The mobile phase gradient used was 50:50 (Solvent A:Sovlent B) to 3:97 (Solvent A:Solvent B) over 12 minutes. The qTOF MS parameters were set as follows: mass range, 50-1000 m/z; gas temperature, 350 C, drying gas flow rate, 11 L/min, nebulizer, 35 psig.

E. coli Assays

MCA fluorescence in *E. coli* (DH5α strain) was measured as described previously (Yapici *et al*). Briefly, *E. coli* was transformed with a plasmid allowing LacI-inducible expression of an empty vector (control), PATL3, or TIL. Cells at OD_{600} were treated with IPTG and grown for 6 hours at 37º C. Cells were treated with 10 μM merocyanine for 30 minutes, and then imaged using a dsRED imaging set up on a fluorescence microscope. For apocarotenoid binding experiments, cells were incubated with IPTG for 6 hours at 37º C, then pre-treated with 200 μM retinal or 200

μM anchorene for 30 minutes. Following this, cells were treated with 10 μM merocyanine and then imaged.

Statistical Analysis.

For all experiments with more than two samples, data was analyzed using one-way ANOVAs with Tukey's multiple comparison tests. All experimental analyses have a one-way ANOVA p value ≤ 0.05. For experiments with two samples, data were analyzed using unpaired t-tests. The symbols *, **, ***, and **** indicate p values ≤ 0.05, 0.01, 0.001, and 0.0001, respectively. Unless otherwise stated, graphs show all biological replicates which were collected over the course of 3 or more technical replicates. All box and whisker plots show the minimum to maximum range of data points. All error bars in bar graphs show standard deviation.

Synthesis and Characterization of Merocyanine Aldehyde (MCA)

General Materials and Methods

Unless stated otherwise, reactions were conducted in oven-dried glassware under an atmosphere of nitrogen or argon using anhydrous solvents (passed through activated alumina columns). All commercially obtained reagents were used as received. Flash column chromatography was performed using silica on a CombiFlash® Rf 200i (Teledyne Isco, Inc.). High-resolution LC/MS analyses were conducted on a Thermo-Fisher LTQ-Orbitrap-XL hybrid mass spectrometer system with an Ion MAX API electrospray ion source in negative ion mode. Analytical LC/MS was performed using a Shimadzu LCMS-2020 Single Quadrupole utilizing a Kinetex 2.6 μm C18 100 Å (2.1 x 50 mm) column obtained from Phenomenex, Inc. Runs employed a gradient of 0→90% MeCN/0.1% aqueous formic acid over 4.5 min at a flow rate of 0.2 mL/min. ^{1}H NMR and ^{13}C NMR spectra were recorded on Bruker spectrometers (at 400 or 500 MHz or at 100 or 125 MHz) and are reported relative to deuterated solvent signals. Data for ^{1}H NMR spectra are reported as follows: chemical shift (δ ppm), multiplicity, coupling constant (Hz), and integration. Data for ^{13}C NMR spectra are reported in terms of chemical shift. Absorption curves were performed on a Shimadzu UV-2550 spectrophotometer operated by UVProbe 2.32 software. Fluorescence traces were recorded on a PTI QuantaMaster steady-state spectrofluorimeter operated by FelixGX 4.2.2 software, with 5 nm excitation and emission slit widths, 1.0 s integration rate, and emission correction enabled. Data analysis and curve fitting were performed using MS Excel 2016 and GraphPad Prism 8.

Synthetic Procedures

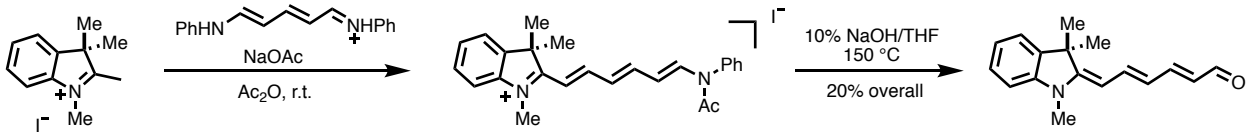

S1 **MeroCy Aldehyde**

Intermediate S1. 1,2,3,3-Tetramethyl-3H-indolium iodide (301 mg, 1 mmol), glutaconaldehydedianil hydrochloride (284 mg, 1 mmol, 1 equiv.), NaOAc (172 mg, 2.1 mmol, 2.1 equiv) and acetic anhydride (12 mL) were added to a scintillation vial equipped with a magnetic stir bar. The reaction mixture was stirred at room temperature for 0.5 h. When the starting material was consumed (reaction control: LC-MS), the reaction mixture was divided into two portions and precipitated into Et_2O (30 x 2 mL) in two falcon tubes. The dark purple suspension was centrifuged for 5 min at 4500 RPM and the supernatant decanted. Each pellet

was resuspended in Et_2O (30 mL), the centrifugation process was repeated, and the pellets were dried under vacuum for 1 h (< 0.1 Torr). The crude product was purified by automated flash chromatography (40 g silica, 0 → 15% MeOH/CH_2Cl_2) to afford the known intermediate **S1** as a purple solid in 66% yield (331 mg) with spectroscopic data in agreement with that reported in the literature *(20)*. ^{1}H NMR (400 MHz, $CDCl_3$) δ 8.17 (d, *J* = 13.7 Hz, 1H), 7.85 (dd, *J* = 15.0, 11.3 Hz, 1H), 7.62 – 7.45 (m, 8H), 7.22 – 7.15 (m, 3H), 6.90 (dd, *J* = 14.4, 11.2 Hz, 1H), 5.41 (dd, *J* = 13.7, 11.4 Hz, 1H), 4.22 (s, 3H), 1.97 (s, 3H), 1.72 (s, 6H) ppm; ^{13}C NMR (100 MHz, $CDCl_3$) δ 180.66, 169.51, 156.06, 151.82, 142.65, 141.66, 141.24, 138.02, 130.84, 130.21, 130.04, 129.56, 128.99, 128.23, 122.51, 114.04, 113.79, 113.64, 77.48, 77.16, 76.84, 51.57, 36.09, 27.24, 23.48 ppm.

MeroCy Aldehyde. Intermediate **S1** (331 mg) was dissolved in THF (6.7 mL) and treated with 10% NaOH (20 mL) and heated to 150 °C in a sealed microwave vial for 18 h, during which time the reaction mixture changed color from purple to yellow. The reaction mixture was allowed to cool and was extracted with CH_2Cl_2 (3 x 20 mL). The combined organic layer was dried over Na_2SO_4, concentrated by rotary evaporation, and purified by automated flash chromatography (12 g silica, 0 → 50% EtOAc/hexanes) to afford **MeroCy Aldehyde** in 20% yield (50 mg) as an orange-brown solid. ^{1}H NMR (400 MHz, DMSO-d6) δ 9.39 (d, *J* = 8.3 Hz, 1H), 7.54 – 7.43 (m, 2H), 7.31 (d, *J* = 7.3, 1.2 Hz, 1H), 7.19 (t, *J* = 7.7, 1.2 Hz, 1H), 6.94 – 6.84 (m, 2H), 6.23 (dd, *J* = 13.9, 11.5 Hz, 1H), 5.91 (dd, *J* = 14.7, 8.3 Hz, 1H), 5.55 (d, *J* = 12.5 Hz, 1H), 3.19 (s, 3H), 1.55 (s, 6H) ppm; ^{13}C NMR (100 MHz, DMSO-d6) δ 192.38, 162.33, 155.50, 144.17, 141.84, 138.86, 127.79, 124.61, 121.69, 121.42, 120.53, 107.29, 96.46, 45.86, 40.15, 39.94, 39.73, 39.52, 39.31, 39.10, 38.89, 29.08, 27.81 ppm; HR-MS (ESI) calculated for $C_{17}H_{19}NO$ $(M+H)^+$ 254.1539, observed 254.1530.

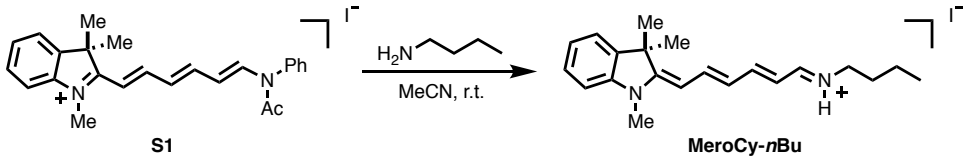

S1 **MeroCy-*n*Bu**

MeroCy-*n*Bu. S1 (9.0 mg, 0.018 mmol) was dissolved in dry MeCN (200 µL) in a 1-dram vial equipped with a magnetic stir bar and the solution was flushed with nitrogen. *n*-butylamine (11.9 µL, 0.12 mmol, 5 equiv.) was added under nitrogen and the reaction mixture was stirred for 5 minutes, during which time the color changed from red to magenta and LC-MS analysis indicated full conversion to the *n*-butylamine adduct. The reaction mixture was evaporated by nitrogen stream, and the crude residue was purified by automated flash chromatography (4 g silica, 0 → 15% MeOH/CH_2Cl_2) to afford **MeroCy-*n*Bu** in 87% yield (6.3 mg) as a magenta film. The ^{1}H NMR spectrum of **MeroCy-*n*Bu** indicates the presence of a mixture of isomers, as described for a similar compound *(21)*. See below for optical characterization.

Determination of Molar Absorption **Coefficients**

Molar absorption coefficients (ε) were determined in MeCN using Beer's law, from plots of absorbance vs. concentration. Measurements were performed in 10 mm path length quartz cuvettes (Hellma 111-QS), maintained at 25 °C, with absorbance at the highest concentration ≤ 1.0.

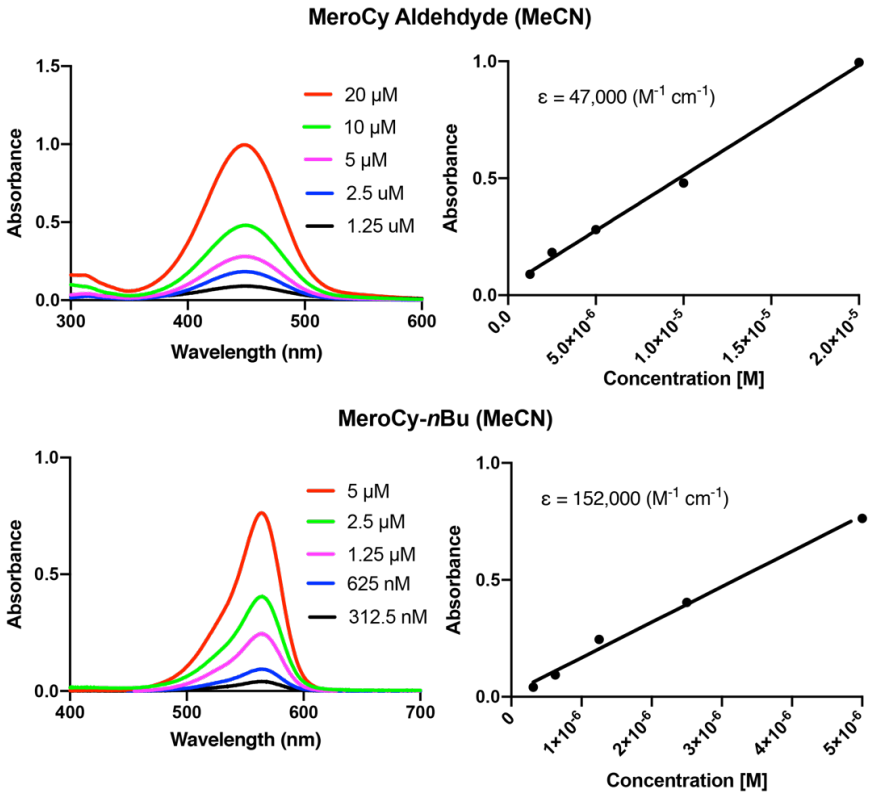

Left: Absorbance spectra of the compounds indicated in MeCN. Right: Absorbance values at λ_{max} as a function of concentration. The slope of the line corresponds to the molar absorption coefficient ε.

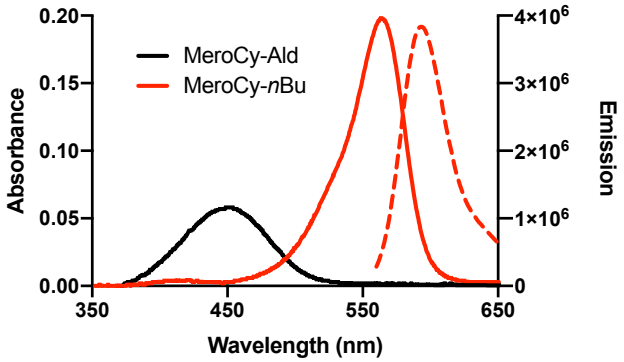

Absorbance (solid lines) and emission spectra ($\lambda_{excitation}$ = 520 nm, dashed line) of the compounds indicated at a concentration of 1 µM in MeCN.

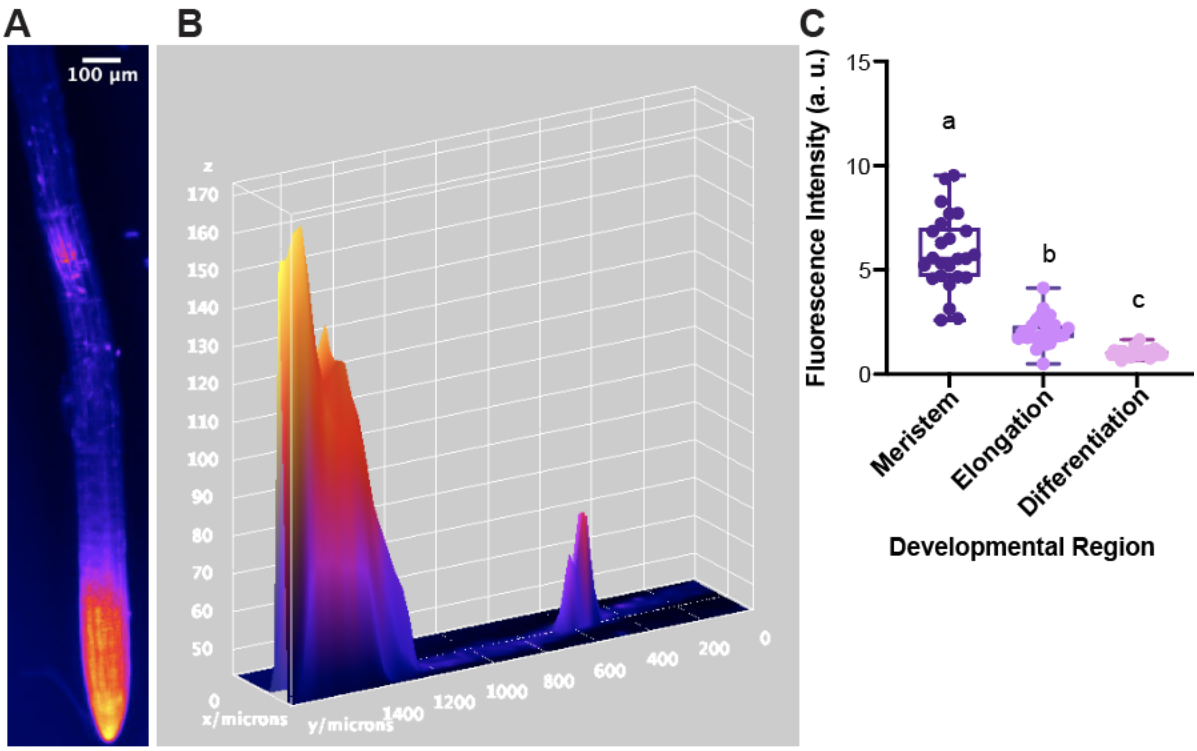

Fig. S1.

Merocyanine aldehyde (MCA) treatment of Arabidopsis roots reveals spatial and temporal dynamics of plant retinoid-binding proteins. A) A representative image of a root treated with MCA. B) A 3D surface plot shows the signal intensity profile of the root shown in panel A. C) MCA fluorescence intensity in root meristems, elongation zones, and differentiation zones that are not experiencing an MCA oscillation.

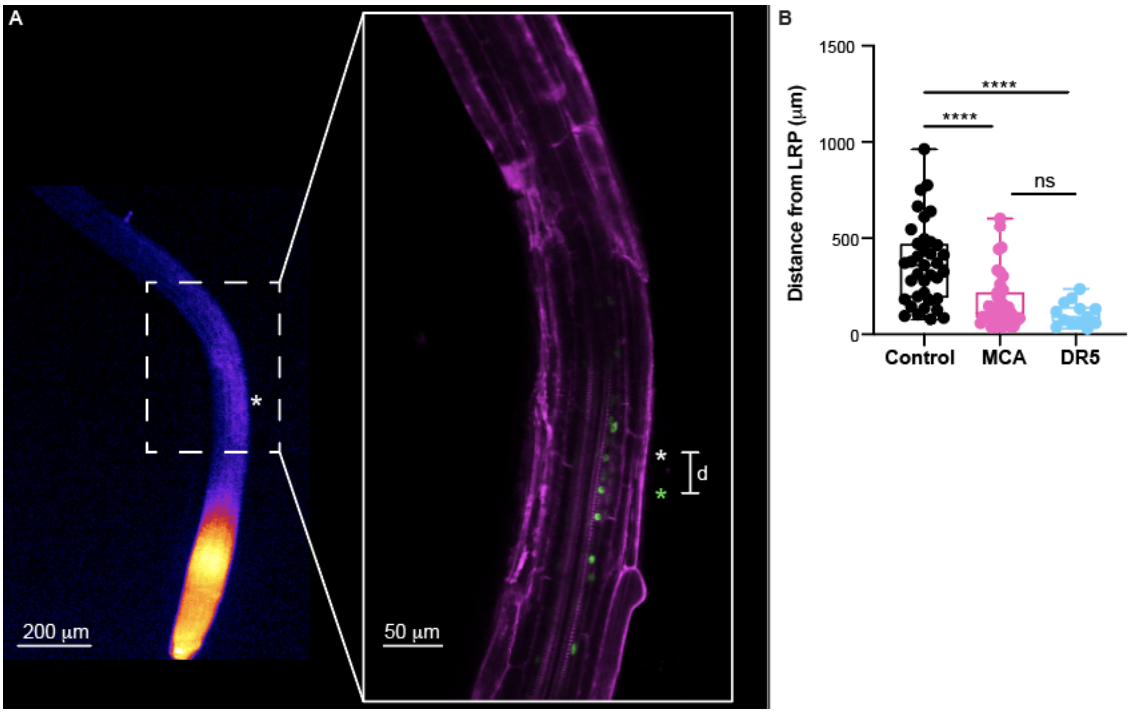

Fig. S2.

Tracking MCA pulses over time in *pGATA23:GFP* roots *(22).* A) In order to characterize the physical relationship between the site of MCA oscillations and lateral root primordia, we tracked roots over the course of several days using fluorescence microscopy. The white asterisks indicate the sites of MCA oscillation maxima. The green asterisk indicates the center of a lateral root primordium, identified two days after MCA imaging. B) The distance between the site of maximal MCA fluorescence and the center of the new lateral root primordium was measured to determine how accurately the MCA pulse predicted the location of the lateral root primordium. All MCA, pDR5:LUC root clock, and lateral root primordia sites were chosen without referencing each other. The control site was chosen using a random number generator that was linked to a position in the developing root, and the LRP sites were chosen blindly (without referencing other fluorescence/luminescence channels).

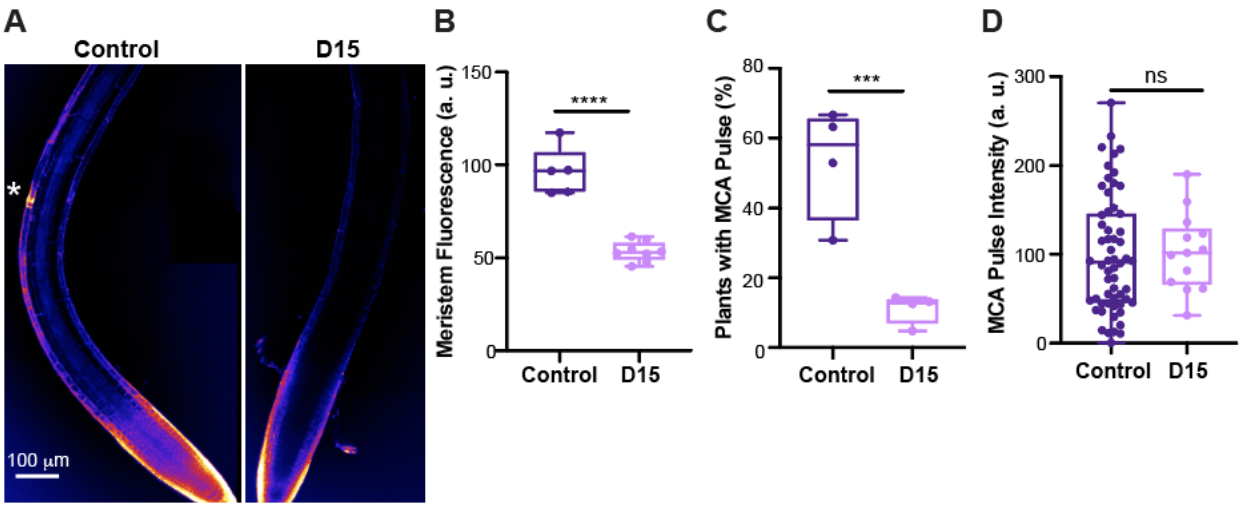

Fig. S3.

MCA fluorescence is affected by D15 treatment. A) Confocal images of MCA fluorescence in control and D15 treated roots (experiment was performed over 1 technical replicate). * indicates the site of a fluorescent pulse in the root. B) Quantification of meristematic MCA fluorescence in control and D15 treated roots. Data points shown are averages of four technical replicates. C) Percent of roots with early differentiation zone MCA oscillations in control and D15 treated plants. D) Fluorescence intensity of MCA pulses in control and D15 treated roots.

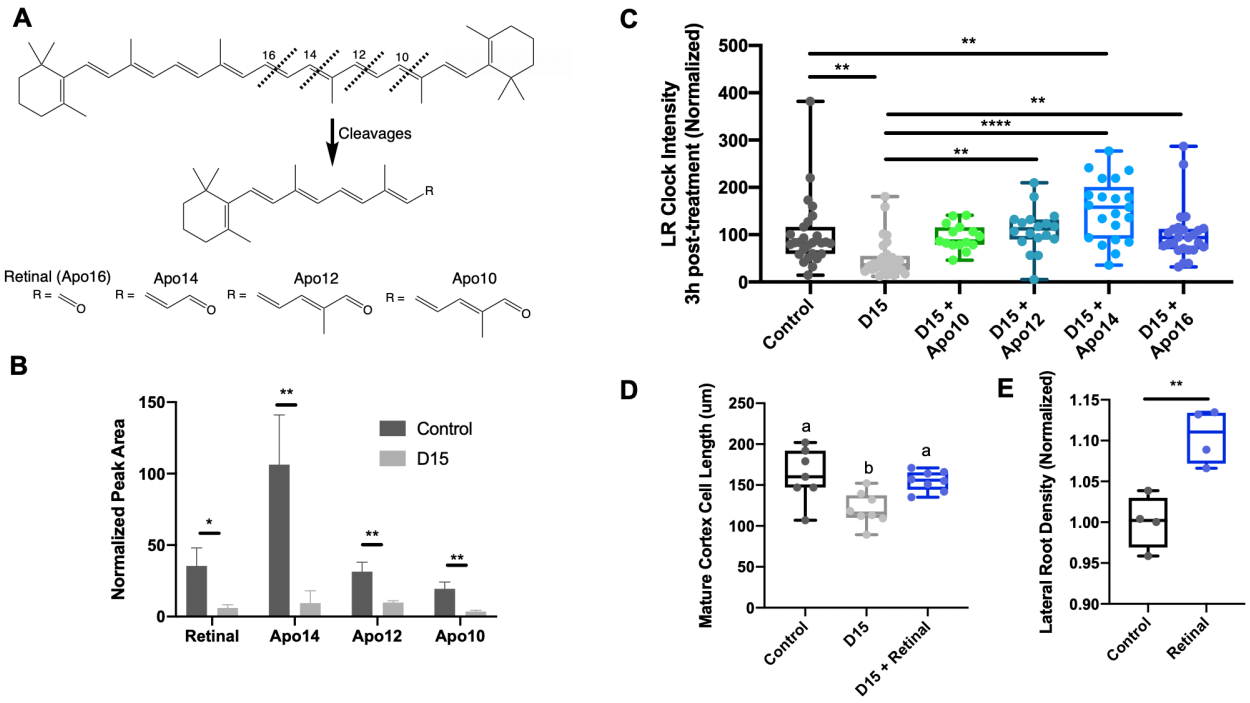

Fig. S4.

Certain apocarotenals can rescue D15 treatment phenotypes. A) Chemical structures of beta-carotene and its apocarotenal cleavage products produced by cleaving the double bonds before the 10th and 16th carbons. B) Relative amount (as measured by HPLC chromatogram peak area) of four apocarotenals in control and D15 treated plants. Peak area was normalized to the peak area of linoleic acid in each sample. C) Maximum intensity of the root clock as measured by DR5 expression in plants treated with D15 and apocarotenals. D) Cell length of mature cortex cells in plants treated with D15 and retinal. E) Lateral root density in control and retinal treated plants (the data points shown are the averages of four experiments).

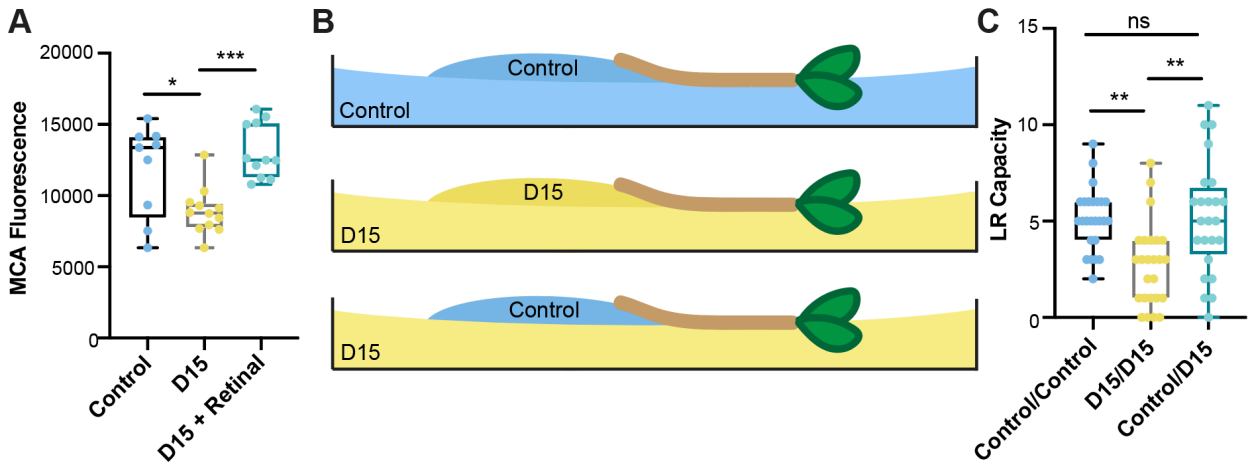

Fig. S5.

The local effects of D15 and retinal on lateral root development. A) Quantification of MCA fluorescence in the root meristem with D15 and retinal treatments. B) Schematic showing how localized D15 treatments were performed. Root tips were selectively exposed to control or D15 treatments. C) Quantification of lateral root (LR) capacity in the experiment shown in panel B. Isolating the root tip from direct D15 treatment (Control/D15) is sufficient to rescue LR capacity.

A

Score	Expect	Method	Identities	Positives	Gaps
24.3 bits(51)	9e-04	Compositional matrix adjust.	35/142(25%)	55/142(38%)	30/142(21%)

```
Query  7    MEVVKGLNVERYMGRWYEIASFP--SRFQPKNGVDTRATYTLNPDGTIHVLNETWSNGKR  64
            +V +   +  RY G WY +A       F    N V    A +T++ +G +        + G+
Sbjct  30   FKVKENFDKNRYSGTWYAMAKKDPEGLFLQDNVV---AQFTVDENGQMSAT----AKGRV  82

Query  65   GFIEGSAYKAD------PKSDEAKLKVKFY-VPPFLPIIPVTGDYWVLYIDPDYQHALI-  116
                       AD          D AK K+K++ V   FL        D+WV   +D DY     +
Sbjct  83   RLFNNWDVCADMIGSFTDTEDPAKFKMKYWGVASFLQ--KGNDDHWV--VDTDYDTYALH  138

Query  117  ---------GQPSRSYLWILSR  129
                    G   + SY ++ SR
Sbjct  139  YSCRELNEDGTCADSYSFVFSR  160
```

B

Fig. S6.

Protein homology between *A. thaliana* TIL and *G. gallus* RBP4. A) Sequence alignment procured using the National Center for Biotechnology Information (NCBI) protein Basic Local Alignment Search Tool (BLAST). B) Overlay of predicted protein structures of *A. thaliana* TIL (rainbow) and *G. gallus* RBP4 (purple) using iTASSER.

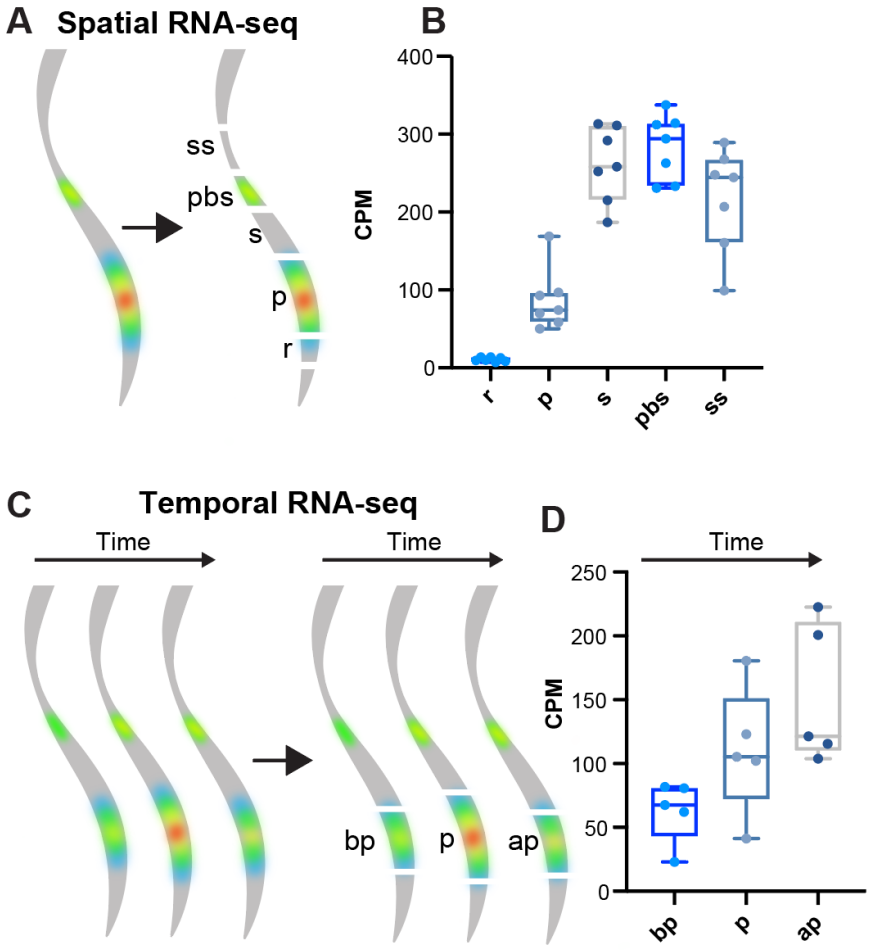

Fig. S7.

RNA-seq experiments reveal TIL oscillations during the root clock. Data and root schematics are adapted from Wachsman *et al (17)*. A) Schematic showing the experimental procedure. Roots were dissected into five regions at the time of DR5 oscillation maxima: the region rootward of the oscillation ("r"), the oscillation region ("p"), the region directly shootward of the oscillation ("s"), the most recently formed pre-branch site ("pbs") marking the cells undergoing organogenesis, and the region immediately shootward of the new pre-branch site ("ss"). B) Gene expression (in counts per million) of TIL in different regions of the root undergoing the maxima of DR5 oscillations (*2*). C) Schematic of a temporal experiment performed in Wachsman *et al (17)*. The root zones experiencing DR5 oscillations were dissected at three time points: before the DR5 oscillation maxima ("bp"), during the oscillation maxima ("p"), and after the oscillation maxima ("ap"). D) Gene expression (in counts per million) of TIL during root clock oscillations (*2*).

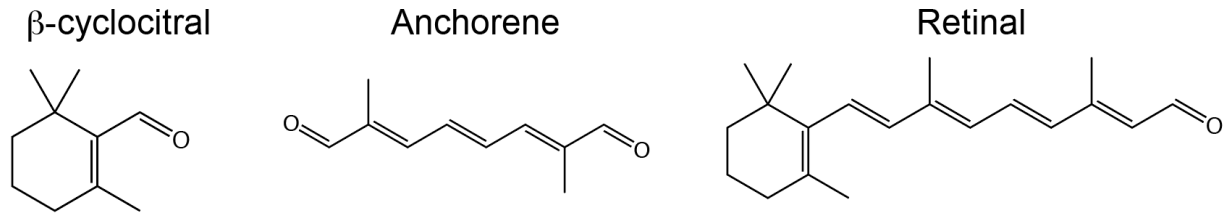

Fig. S8.

Chemical structures of three apocarotenals: β-cyclocitral, anchorene ((2E,4E,6E)-2,7-dimethylocta-2,4,6-trienedial), and retinal.

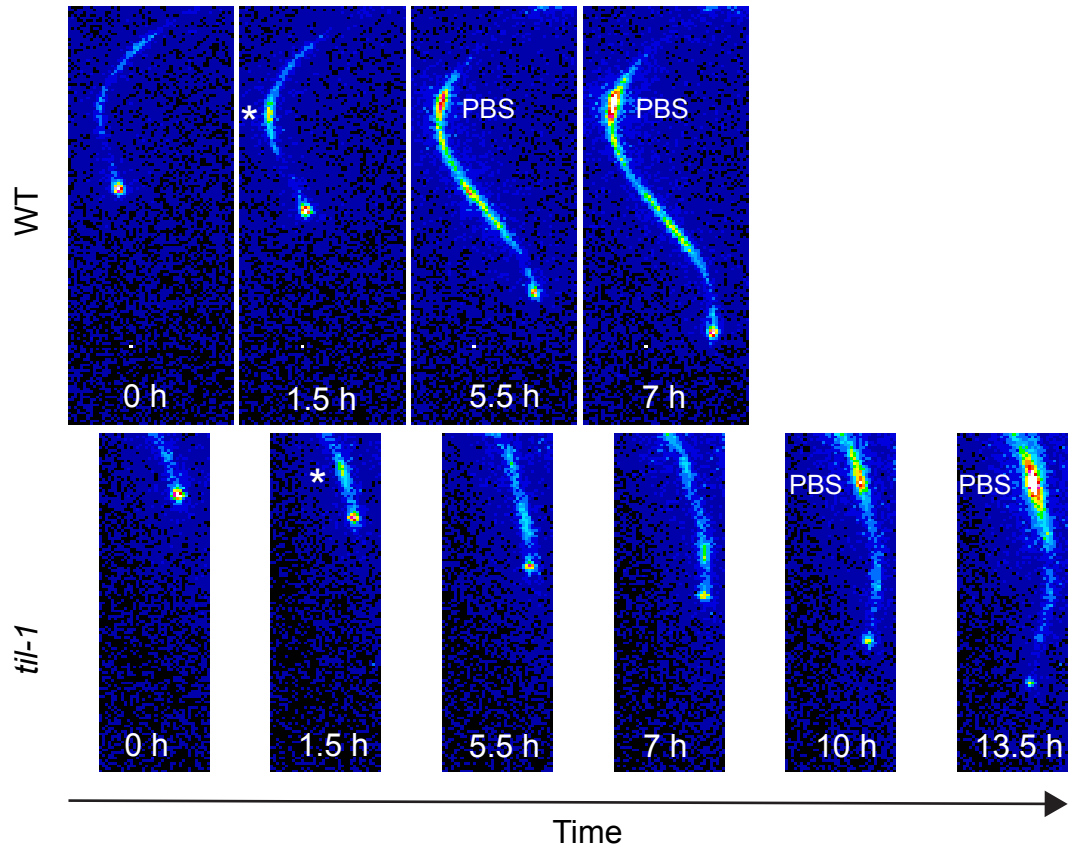

Fig. S9.

Time course of *pDR5:LUC* root clock oscillations in WT and *til-1* (see Movie S3 for full time course). * marks the maximum DR5 oscillation, which was normalized to occur at 1.5 hours for each root. The first timepoints when the corresponding pre-branch sites (PBS) were clearly visible are shown for each root. In WT, this occurred at 5.5 h. In *til-1*, this occurred at 10 h.

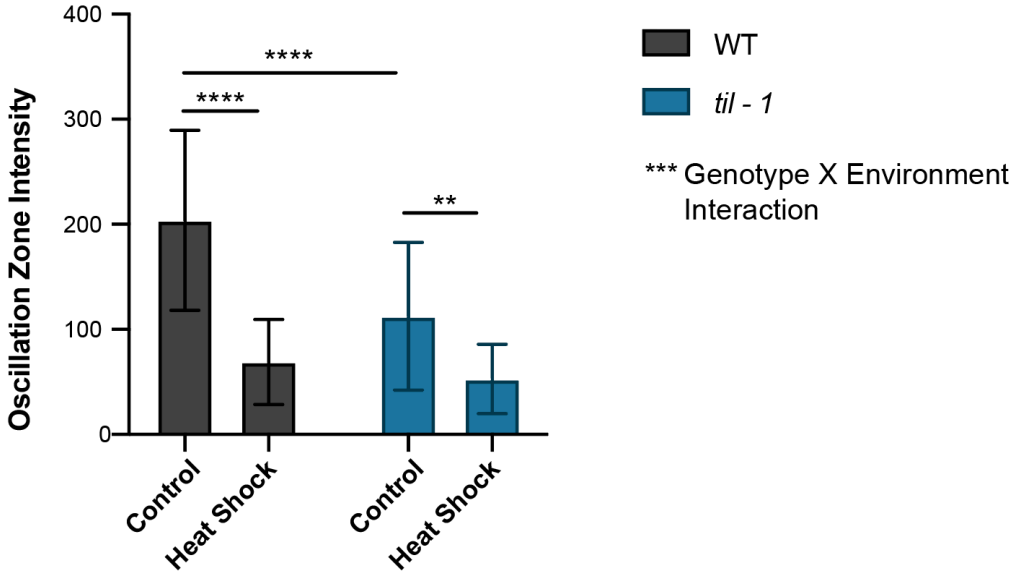

Fig. S10.

Graph showing the luminescence intensity in the root clock oscillation zone of pDR5:LUC plants during control and heat shock conditions. Seedlings were then subjected to heat treatment at 45°C heat shock for 1 hour. The genotype by environment interaction was statistically significant (p value = 0.008). For each replicate, n > 27 plants.

Supplementary Movies

Movie S1. MCA fluorescence dynamics in a growing root. The scale bar is 200 mm. The duration of the movie is 15 hours. The images in this movie have been corrected for photobleaching using the ImageJ Histogram Matching algorithm.

Movie S2. The root clock in *pDR5:LUC* plants treated with D15. One hour before imaging, roots were treated with a vehicle control (left) or retinal (right). The scale bar is 0.5 mm. The movie covers a period of 8 hours.

Movie S3. The *pDR5:LUC* root clock and pre-branch site formation in WT and *til-1* plants. The root on the left is WT and the root on the right is *til-1*. The scale bar is 0.5 mm.
The movie covers a period of 13.5 hours.

Movie S4. A representative *pTIL:LUC* root. The scale bar is 1 mm. The movie covers a period of 12 hours.

References and Notes

1. M. A. Moreno-Risueno, J. M. Van Norman, A. Moreno, J. Zhang, S. E. Ahnert, P. N. Benfey, Oscillating gene expression determines competence for periodic *Arabidopsis* root branching. *Science* **329**, 1306–1311 (2010). doi:10.1126/science.1191937 Medline

2. W. Xuan, H. De Gernier, T. Beeckman, The dynamic nature and regulation of the root clock. *Development* **147**, dev181446 (2020). doi:10.1242/dev.181446 Medline

3. A. J. Dickinson, K. Lehner, J. Mi, K.-P. Jia, M. Mijar, J. Dinneny, S. Al-Babili, P. N. Benfey, β-Cyclocitral is a conserved root growth regulator. *Proc. Natl. Acad. Sci. U.S.A.* **116**, 10563–10567 (2019). doi:10.1073/pnas.1821445116 Medline

4. J. M. Van Norman, J. Zhang, C. I. Cazzonelli, B. J. Pogson, P. J. Harrison, T. D. H. Bugg, K. X. Chan, A. J. Thompson, P. N. Benfey, Periodic root branching in *Arabidopsis* requires synthesis of an uncharacterized carotenoid derivative. *Proc. Natl. Acad. Sci. U.S.A.* **111**, E1300–E1309 (2014). doi:10.1073/pnas.1403016111 Medline

5. K. P. Jia, A. J. Dickinson, J. Mi, G. Cui, T. T. Xiao, N. M. Kharbatia, X. Guo, E. Sugiono, M. Aranda, I. Blilou, M. Rueping, P. N. Benfey, S. Al-Babili, Anchorene is a carotenoid-derived regulatory metabolite required for anchor root formation in *Arabidopsis*. *Sci. Adv.* **5**, eaaw6787 (2019). doi:10.1126/sciadv.aaw6787 Medline

6. C. Ruyter-Spira, W. Kohlen, T. Charnikhova, A. van Zeijl, L. van Bezouwen, N. de Ruijter, C. Cardoso, J. A. Lopez-Raez, R. Matusova, R. Bours, F. Verstappen, H. Bouwmeester, Physiological effects of the synthetic strigolactone analog GR24 on root system architecture in Arabidopsis: Another belowground role for strigolactones? *Plant Physiol.* **155**, 721–734 (2011). doi:10.1104/pp.110.166645 Medline

7. J. Agusti, S. Herold, M. Schwarz, P. Sanchez, K. Ljung, E. A. Dun, P. B. Brewer, C. A. Beveridge, T. Sieberer, E. M. Sehr, T. Greb, Strigolactone signaling is required for auxin-dependent stimulation of secondary growth in plants. *Proc. Natl. Acad. Sci. U.S.A.* **108**, 20242–20247 (2011). doi:10.1073/pnas.1111902108 Medline

8. I. De Smet, L. Signora, T. Beeckman, D. Inzé, C. H. Foyer, H. Zhang, An abscisic acid-sensitive checkpoint in lateral root development of *Arabidopsis*. *Plant J.* **33**, 543–555 (2003). doi:10.1046/j.1365-313X.2003.01652.x Medline

9. M. B. Wahl, C. Deng, M. Lewandoski, O. Pourquié, FGF signaling acts upstream of the NOTCH and WNT signaling pathways to control segmentation clock oscillations in mouse somitogenesis. *Development* **134**, 4033–4041 (2007). doi:10.1242/dev.009167 Medline

10. J. Vermot, O. Pourquié, Retinoic acid coordinates somitogenesis and left-right patterning in vertebrate embryos. *Nature* **435**, 215–220 (2005). doi:10.1038/nature03488 Medline

11. M. Maden, Retinoic acid in the development, regeneration and maintenance of the nervous system. *Nat. Rev. Neurosci.* **8**, 755–765 (2007). doi:10.1038/nrn2212 Medline

12. S. C. Lin, P. Dollé, L. Ryckebüsch, M. Noseda, S. Zaffran, M. D. Schneider, K. Niederreither, Endogenous retinoic acid regulates cardiac progenitor differentiation. *Proc. Natl. Acad. Sci. U.S.A.* **107**, 9234–9239 (2010). doi:10.1073/pnas.0910430107 Medline

13. I. Yapici, K. S. S. Lee, T. Berbasova, M. Nosrati, X. Jia, C. Vasileiou, W. Wang, E. M. Santos, J. H. Geiger, B. Borhan, "Turn-on" protein fluorescence: In situ formation of cyanine dyes. *J. Am. Chem. Soc.* **137**, 1073–1080 (2015). doi:10.1021/ja506376j Medline

14. J.-B. F. Charron, F. Ouellet, M. Pelletier, J. Danyluk, C. Chauve, F. Sarhan, Identification, expression, and evolutionary analyses of plant lipocalins. *Plant Physiol.* **139**, 2017–2028 (2005). doi:10.1104/pp.105.070466 Medline

15. W. T. Chi, R. W. M. Fung, H. C. Liu, C. C. Hsu, Y. Y. Charng, Temperature-induced lipocalin is required for basal and acquired thermotolerance in *Arabidopsis*. *Plant Cell Environ.* **32**, 917–927 (2009). doi:10.1111/j.1365-3040.2009.01972.x Medline

16. S. Boca, F. Koestler, B. Ksas, A. Chevalier, J. Leymarie, A. Fekete, M. J. Mueller, M. Havaux, *Arabidopsis* lipocalins AtCHL and AtTIL have distinct but overlapping functions essential for lipid protection and seed longevity. *Plant Cell Environ.* **37**, 368–381 (2014). doi:10.1111/pce.12159 Medline

17. G. Wachsman, J. Zhang, M. A. Moreno-Risueno, C. T. Anderson, P. N. Benfey, Cell wall remodeling and vesicle trafficking mediate the root clock in *Arabidopsis*. *Science* **370**, 819–823 (2020). doi:10.1126/science.abb7250

18. J. G. Dubrovsky, M. Sauer, S. Napsucialy-Mendivil, M. G. Ivanchenko, J. Friml, S. Shishkova, J. Celenza, E. Benková, Auxin acts as a local morphogenetic trigger to specify lateral root founder cells. *Proc. Natl. Acad. Sci. U.S.A.* **105**, 8790–8794 (2008). doi:10.1073/pnas.0712307105 Medline

19. L. A. Kelley, S. Mezulis, C. M. Yates, M. N. Wass, M. J. Sternberg, The Phyre2 web portal for protein modeling, prediction and analysis. *Nat. Protoc.* **10**, 845–858 (2015). doi:10.1038/nprot.2015.053 Medline

20. M. Y. Berezin, K. Guo, B. Teng, W. B. Edwards, C. J. Anderson, O. Vasalatiy, A. Gandjbakhche, G. L. Griffiths, S. Achilefu, Radioactivity-synchronized fluorescence enhancement using a radionuclide fluorescence-quenched dye. *J. Am. Chem. Soc.* **131**, 9198–9200 (2009). doi:10.1021/ja903685b

21. L. Herwig, A. J. Rice, C. N. Bedbrook, R. K. Zhang, A. Lignell, J. K. B. Cahn, H. Renata, S. C. Dodani, I. Cho, L. Cai, V. Gradinaru, F. H. Arnold, Directed evolution of a bright near-infrared fluorescent rhodopsin using a synthetic chromophore. *Cell Chem. Biol.* **24**, 415–425 (2017). doi:10.1016/j.chembiol.2017.02.008 Medline

22. B. De Rybel, V. Vassileva, B. Parizot, M. Demeulenaere, W. Grunewald, D. Audenaert, J. Van Campenhout, P. Overvoorde, L. Jansen, S. Vanneste, B. Möller, M. Wilson, T. Holman, G. Van Isterdael, G. Brunoud, M. Vuylsteke, T. Vernoux, L. De Veylder, D. Inzé, D. Weijers, M. J. Bennett, T. Beeckman, A novel Aux/IAA28 signaling cascade activates GATA23-dependent specification of lateral root founder cell identity. *Curr. Biol.* **20**, 1697–1706 (2010). doi:10.1016/j.cub.2010.09.007 Medline